Journal of Extracellular Biology

RESEARCH ARTICLE OPEN ACCESS

Direct Experimental Evidence for Selective Uptake of Function-Specific Small Extracellular Vesicles by Recipient Cells

Yuhong Liu[1] | Natsumi Tiffany Ishii[1] | Jun-Yu Dong[1] | Yaqi Zhao[1] | Yingdong Luo[1] | Zhuhui Ren[1] | Tianben Ding[1] | Tamako Nishimura[2] | Ryo Iizuka[3] | Akihiro Isozaki[1,4] | Sotaro Uemura[3] | Shiro Suetsugu[2,5,6,7] | Keisuke Goda[1,8,9,10]

[1]Department of Chemistry, The University of Tokyo, Tokyo, Japan | [2]Division of Biological Science, Nara Institute of Science and Technology, Ikoma, Japan | [3]Department of Biological Sciences, The University of Tokyo, Tokyo, Japan | [4]Department of Mechanical Engineering, Ritsumeikan University, Kusatsu, Japan | [5]Data Science Center, Nara Institute of Science and Technology, Ikoma, Japan | [6]Center of Digital Green-Innovation, Nara Institute of Science and Technology, Ikoma, Japan | [7]Medilux Research Center, Nara Institute of Science and Technology, Ikoma, Japan | [8]International Center for Synchrotron Radiation Innovation Smart (SRIS), Tohoku University, Miyagi, Japan | [9]The Institute of Technological Sciences, Wuhan University, Wuhan, China | [10]Department of Bioengineering, University of California Los Angeles, Los Angeles, USA

Correspondence: Tianben Ding (tding@g.ecc.u-tokyo.ac.jp) | Keisuke Goda (goda@chem.s.u-tokyo.ac.jp)

Received: 20 May 2025 | **Revised:** 14 August 2025 | **Accepted:** 9 September 2025

Funding: This work was mainly supported by JSPS Core-to-Core Program JPJSCCCA20190007 (K.G.), JSPS KAKENHI JP20H00317 (K.G.), JP23KJ0430 (Y.L.), JP24K17800 (T.D.), JP23H02476 (T.N.), JP24H01286 and JP24K02024 (S.S.), JST ASPIRE Program JPMJAP2316 (K.G.), JST CREST JPMJCR1863 and JPMJCR24B3 (S.S.), Mazda Foundation (T.D.) and KAKETSUKEN (K.G.). Additional support was provided by supported by the Mohammed bin Salman Center for Future Science and Technology for Saudi-Japan Vision 2030 (K.G.), the Cell Aging Control Endowed Chair at the University of Tokyo (K.G.) and the Nanotechnology Platform Project by the Ministry of Education, Culture, Sports, Science and Technology of Japan JPMXP09A21UT0014.

Keywords: biological functions | cell discernment | subpopulation isolation

ABSTRACT

Small extracellular vesicles (sEVs), ranging from 30 to 200 nm in diameter, are a subset of extracellular vesicles that play an essential role in intercellular communication by transporting bioactive molecules between cells. Due to their diverse cargo and origins, sEVs form a highly heterogeneous population. Previous studies have suggested that recipient cells uptake specific sEVs to ensure accurate signalling, but direct experimental evidence on how cells effectively communicate in such a complex and noisy environment has been lacking. In this study, we provide direct experimental evidence by developing a method to retrieve and analyze internalized sEVs from the intracellular membrane compartments of recipient cells. Using this sEV retrieval method, we isolated sEV subpopulations from two types of breast cancer cells after incubation with sEVs derived from mixed cell cultures. We then assessed their functional roles by evaluating the phenotypic responses of cells treated with these retrieved sEV subpopulations. Our results reveal apparent differences in their functional impacts, indicating that cells employ a function-based mechanism to selectively uptake sEVs. This finding advances our understanding of how cells enhance communication efficiency via sEVs. Further investigation into this phenomenon could offer deeper insights into intercellular communication and its role in health and disease.

This is an open access article under the terms of the Creative Commons Attribution-NonCommercial License, which permits use, distribution and reproduction in any medium, provided the original work is properly cited and is not used for commercial purposes.

© 2025 The Author(s). *Journal of Extracellular Biology* published by Wiley Periodicals, LLC on behalf of the International Society for Extracellular Vesicles.

1 | Introduction

Small extracellular vesicles (sEVs) are a smaller fraction of extracellular vesicles (EVs) released from cells into the extracellular space. Measuring between 30 and 200 nm in diameter, sEVs carry an assortment of biologically active molecules, including proteins, lipids, RNAs and DNAs, which play critical roles in intercellular communication (Pluchino and Smith 2019; van Niel et al. 2018). A wide diversity of sEVs is released by different cell types, or even the same type of cells, indicating a highly heterogeneous population of sEVs within the extracellular space (van de Wakker et al. 2023; Bordanaba-Florit et al. 2021; Kowal et al. 2016; Tosar et al. 2015). This heterogeneity stems from distinct mechanisms of vesicle formation: bioactive molecules such as non-coding and coding RNAs, signalling molecules and membrane-bound receptors can be packaged into ectosomes via direct budding from the plasma membrane or into exosomes through endosomal sorting before being released (Dixson et al. 2023; Sung et al. 2021; Yu et al. 2021).

How cells effectively communicate in a highly heterogeneous or noisy environment remains a central question in biology. Observational studies suggest that recipient cells selectively internalize preferred sEVs to facilitate long-distance communication (Mathieu et al. 2019; Kalluri and LeBleu 2020; Montecalvo et al. 2012; Chen et al. 2018; Qiu et al. 2021; Nabet et al. 2017; Cheng et al. 2023; Hoshino et al. 2015; Wen et al. 2016; Urabe et al. 2023). For example, PD-1 positive CD8 T cells interact with exosomes expressing PD-L1, potentially modulating immune responses (Chen et al. 2018), while triple-negative breast cancer cells absorb sEVs from stromal fibroblasts, carrying RNAs that activate STAT1, contributing to therapy resistance (Nabet et al. 2017). Similarly, pre-metastatic sites in mice accumulate cancer-derived sEVs in a process referred to as targeted biodistribution (Hoshino et al. 2015; Zomer et al. 2015).

While these observations provide valuable insights, direct experimental evidence for the selective uptake of sEVs by recipient cells remains absent. Most previous studies have explored specific sEV-recipient interactions without considering how cells navigate a diverse sEV environment. Ligand-receptor interactions (Chen et al. 2018; Wang et al. 2024; Ivanova et al. 2023), though effective for a limited subset of sEVs, do not fully explain this selectivity. Proposed mechanisms such as clathrin-mediated endocytosis, phagocytosis, macropinocytosis, lipid rafts and filopodia-mediated uptake (He et al. 2023; Fuentes et al. 2020; Ben-Aicha et al. 2024; Costa Verdera et al. 2017; Peruzzi et al. 2024; Rilla 2021; Mulcahy et al. 2014) lack direct evidence for specificity in sEV selection. Clarifying how cells differentiate and internalize specific sEVs within a complex environment is crucial for advancing our understanding of intercellular communication.

In this study, we provide direct experimental evidence supporting the selective uptake of sEVs by recipient cells by developing a method to retrieve and analyze internalized sEVs from the intracellular membrane compartments of these cells. Using differential ultracentrifugation, we isolated all nanometer-scale particles from the recipient cells following sEV internalization. Subsequent analysis allowed us to evaluate the content of these vesicles and validate the functional diversity among sEV subpopulations in the phenotypic expression of cells. We observed apparent differences ($p < 0.05$) in the phenotypic response of different cell types, indicating that recipient cells employ a mechanism for function-based selection of sEVs. This mechanism potentially enhances the efficiency in sEV-mediated cell-cell communication.

2 | Materials and Methods

2.1 | Materials

Cell line, reagents, equipment, and other resources are listed in Table S1.

2.2 | Cell Culture

Cells from the fibroblast cell line MRC5, human breast cancer cell line MCF7, and triple-negative breast cancer cell line MDA-MB-436 were cultured in Dulbecco's Modified Eagle's Medium (DMEM, Fujifilm) supplemented with 10% exosome-depleted foetal bovine serum (FBS, ThermoFisher) and 1% penicillin-streptomycin (Fujifilm). The cells were passaged using 0.5% trypsin-EDTA (Fujifilm) at 80% confluency. Cocultures were utilized for sEV isolation, MDA-MB-436 cells were mixed at a 1:1 ratio with MRC5 cells and harvested for 96 h to condition the medium. The viability of cell culture was monitored daily by observing cell morphology under a microscope.

2.3 | Isolation of sEVs

sEVs were isolated from the conditioned medium of cocultures according to a previously described protocol (Théry et al. 2006). Briefly, the conditioned medium was centrifuged at 300 *g* for 5 min, 2000 *g* for 15 min and 10,000 *g* for 45 min to remove cells and cell debris. Subsequently, ultracentrifugation was performed at 100,000 *g* for 80 min to collect the sEV pellets. The pellets were then washed with PBS and subjected to another round of ultracentrifugation at 100,000 *g* to eliminate contaminating proteins. The resulting pellet was resuspended in 200 μL of PBS and stored at 4°C for a maximum of 3 days.

2.4 | sEV Uptake Assay

MCF7 and MDA-MB-436 cells (3×10^5 cells) were cultured on glass-bottom culture dishes (3 cm in diameter) and allowed to adhere for 24 h. Subsequently, the cells were incubated with 2 mL PKH67-labelled sEVs (5×10^9 sEVs/mL) for 12, 24, 48 and 72 h. After washing the cells with PBS to remove uninternalized sEVs, confocal microscopy (Olympus) and a microplate reader (ThermoFisher) were utilized to assess the fluorescence intensity and capture images of the cells at each time point to determine the optimal incubation time. Additionally, sEVs were covalently labelled using bio-orthogonal click chemistry as described in a previous study (Song et al. 2020). Briefly, unnatural azide ($-N_3$) groups were introduced to the donor cell surface through Ac4ManNAz (10 μM) incubation for 1 day, followed by the labelling of AZDye 488-conjugated dibenzyl cyclooctene (10 μM) on the donor cell surface via bio-orthogonal click chemistry for an additional day. Click chemistry-labelled sEVs were then incubated with recipient cells for sEV subpopulation

isolation. The concentration of sEV subpopulations was assessed by fluorescence intensity using a microplate reader.

2.5 | Retrieval of sEV Subpopulations from Recipient Cells

MCF7, MDA-MB-436 or NIH/3T3 cells were used as recipient cells to recruit sEV subpopulations. Initially, the sEVs derived from cocultures were incubated with the recipient cells for 2 days, and then gently washed with PBS and subsequently detached using trypsin treatment, enabling the extraction of internalized sEVs. The collected recipient cells were promptly subjected to a freezing step at –20°C for 15 min, prior to their lysis process using a 10% PBS + 0.1% Triton hypotonic solution. For each batch of 10^6 cells, 1 mL of lysis buffer was applied, and the recipient cells were maintained on ice for 15 min to release cell compositions in the cytoplasm. Subsequently, the resulting lysate was sequentially centrifuged at 300 *g* for 10 min, 2000 *g* for 30 min and 10,000 *g* for 1 h to remove the large particles. The supernatant was subjected to ultracentrifugation twice at 100,000 *g* for 90 min to further enrich the sEV fraction. The resultant 100,000 *g* cell pellets were delicately resuspended in 200 μL of PBS for immediate use or stored at 4°C for a maximum duration of 2 days.

2.6 | Nanoparticle Tracking Analysis

The sEVs derived from cocultures and the sEV subpopulations retrieved from recipient cells were prepared using PBS in low-protein binding tubes on ice. The sEV dilutions were aspirated with a 1 mL syringe, and the piston was pushed and pulled five times to suspend the sEVs. The suspended sEVs numbers were measured by NanoSight LM10 instrument (Malvern Panalytical), with 60 s of measurement performed for one field of view and a total of five fields of view measured using the standard method. The obtained results were analyzed using the NanoSight software.

2.7 | Immunoblotting

The sEVs or 100,000 *g* cell pellets were lysed using RIPA buffer (ThermoFisher) and supplemented with protease inhibitors (ThermoFisher) on ice for 30 min to extract total protein. Subsequently, the lysate was centrifuged at 10,000 *g* for 10 min at 4°C to eliminate debris such as nucleic acids. Its supernatant was mixed with loading buffer (ThermoFisher) and then heated at 90°C for 15 min. After that, the proteins were separated on an SDS-PAGE gel (Bio-Rad) at 100 V for 90 min, followed by transfer onto a nitrocellulose membrane. The transferred membranes were blocked using 5% nonfat milk and incubated overnight at 4°C with the primary antibody, followed by incubation with horseradish peroxidase (HRP)-conjugated secondary antibodies for 1 h. Finally, the membranes were imaged using iBright Imaging Systems (ThermoFisher) after applying western ECL substrate (Bio-Rad).

2.8 | Transmission Electron Microscopy

Carbon-coated grids (400-mesh, copper) were first glow-discharged for sample preparation. sEV samples and 100,000 *g* cell pellets after 0.1% Triton X-100 treatment and differential ultracentrifugation (dUC) were loaded onto the grids, then stained with 2% (w/v) uranyl acetate and air-dried. Images were obtained with a JEM-1400 Flash transmission electron microscope (JEOL) at 100 kV.

2.9 | Scanning Electron Microscopy

The morphological features of sEVs were examined with a scanning electron microscope with a cold-field emission gun (Regulus 8230, Hitachi). Samples containing sEV suspensions were deposited onto clean silicon substrates and dried at room temperature. Subsequently, a 5 nm layer of gold was sputtered onto the surface via a magnetron sputtering instrument (MSP-mini, Vacuum Device) to enhance the conductivity of the samples. An electron acceleration voltage of 5 kV was used for imaging.

2.10 | Lipid Content Assay

Lipid content in 100,000 *g* cell pellets was assessed using PKH67 staining. After dUC, cell pellets were resuspended in 200 μL PBS, followed by the addition of 0.2 μL PKH67 (Sigma). The mixture was incubated at room temperature for 10 min. Excess dye was neutralized with exosome-depleted serum and removed via ultracentrifugation. The stained pellets were then collected, and green fluorescence intensity was measured at 502 nm using a microplate reader.

2.11 | Surface-Enhanced Raman Spectroscopy

100,000 *g* of recipient cell pellets (10 μL) were mixed with prepared AuNR colloid (20 μL) and a stock NaCl aqueous solution (1 M, 10 μL) to obtain the enhancement of the Raman signal (Song et al. 2021). Each mixed sample suspension was dropped onto a clean silicon chip with a size of 1 mm × 1 mm and then air dried at room temperature before the Raman spectroscope measurements. The Raman spectra were acquired on a confocal Raman microscope (Renishaw inVia) with an excitation wavelength of 785 nm and a diffraction grating of 1200 lines/mm. Photons for all the Raman spectroscopy measurements were collected using a 50× objective lens with a laser spot diameter of 1 μm with an excitation power of 7 mW for an exposure duration of 2 s. Before recording the spectrum of each sample, the spectrometer was calibrated using the characteristic line of silicon (521 cm^{-1}) as a reference. The Raman spectra were obtained by accumulating 20 scans in all cases, and five spectra were collected per sample at different spots. All the Raman spectra were processed with the baseline subtracted using a software program (WiRE 4.0) embedded in the spectrometer. The spectra of the sEV subpopulation from MCF7 (MDA-MB-436) were obtained by subtracting the spectra of the MCF7 0 h (MDA-MB-436) cell pellet from MCF7 48 h (MDA-MB-436 48 h) cell pellet. The spectra were finally presented by adopting a smoothing based on Savitzky–Golay method to further eliminate the spectral noise (10 points of window, no boundary condition, polynomial of fourth order).

2.12 | Cell Proliferation Assay

Recipient MCF7, MDA-MB-436 or MRC5 cells were seeded in a 96-well plate at a density of 5000 cells/well, 7000 cells/well and 5000 cells/well, respectively. After 24 h, once the cells had adhered to the plate, the culture medium was replaced with 100 μL of medium containing isolated sEVs and exosome-depleted serum (5%). The cells were then cultured continuously for 24 h. Following the respective incubation periods, 10 μL of Cell Counting Kit 8 (CCK-8, Abcam) solution was added to each well, and the plate was further incubated at 37°C for 3 h. Subsequently, absorbance at 450 nm was measured using a microplate reader (ThermoFisher).

2.13 | Wound Healing Assay

MCF7, MDA-MB-436 or MRC5 cells (1×10^6 cells) were inoculated into a 6-well plate, with each well containing 2 mL of exosome-depleted cell culture medium. After 24 h of cell culture, the cells were scratched with a wall, and the floating cells were washed away with PBS. The scratch distance was photographed and recorded with a microscope. Mediums with a concentration of 5×10^9 particles/mL were added to the plate, and an appropriate amount of serum-free fresh medium was used as the control group. After 24 or 48 h, the floating cells were washed off, and the scratch distance was recorded by microscope image analysis using ImageJ software.

2.14 | Colony Formation

MCF7 and MDA-MB-436 cells were seeded in a 6-well cell culture plate at 500 cells/well. After 24 h of cell culture, media with a concentration of 5×10^9 particles/mL were added to the plate and an appropriate amount of medium containing 5% exosome-depleted FBS was used as the control group. The medium was replaced every 4 days, and the cells were cultured continuously until each cell cluster contained more than 50 cells. After fixing the cells with 4% paraformaldehyde (Fujifilm), the cell nuclei were stained with 0.1% crystal violet. The number of clones formed in each group was then counted using ImageJ software.

2.15 | Cellular Morphology Analysis

A schematic of the data acquisition sequence is provided in Supporting Information Appendix, Figure S1. Bright-field microscopy images were acquired and used for cell segmentation. The acquired images were processed using Cellpose, an open-source algorithm for robust cell boundary detection (Stringer et al. 2021). Following segmentation, the Sobel operator was applied to refine the edges of each cell. The cellular perimeter was calculated by multiplying the pixel length by the number of pixels along the detected edges, while the cellular area was obtained by multiplying the actual pixel area by the number of pixels within the segmented region. Pixel length was determined by dividing the actual pixel size of the camera (8 μm) by the system magnification (60×). All analyses were implemented in MATLAB 2023b (MathWorks).

2.16 | Quantification and Statistical Analysis

Statistical analysis was performed using Prism software version 10.2.3. Data were assessed for normal distribution and plotted in the figures as mean ± SD. Differences between two treatment groups were assessed using two-tailed, unpaired Student's *t* tests. Significant differences emerging from the statistical tests are indicated in the figures by $*p < 0.05$, $**p < 0.01$, $***p < 0.001$. Individual statistical analyses performed can be found in the figure legends.

3 | Results

3.1 | Recipient Cells Selectively Uptake sEVs

Before assessing the physiological influence of sEVs shed by donor cells on recipient cells, we first focused on the uptake preferences of recipient cells. This was investigated by incubating a heterogeneous pool of sEVs with different recipient cell types. We generated a heterogeneous pool of sEVs by mixing sEVs derived from the human stromal fibroblast cell line, MRC5 and the basal/triple-negative breast cancer cell line, MDA-MB-436, stained with red and green fluorescent dyes, respectively. We incubated this mixture with two types of breast cancer recipient cells, MCF7 (luminal/ER-positive) and MDA-MB-436, to assess their uptake preference and discernment capabilities (Figure 1A). By using two closely related breast cancer subtypes as recipient cells, we aimed to elucidate the specificity of selective sEV uptake. Through switching the fluorescent dyes and replicating experiments, we observed that MDA-MB-436 cells exhibited a stronger preference for MRC5-derived sEV uptake compared to MCF7 cells. This was evidenced by the ratio of MRC5 sEVs to MDA-MB-436 sEVs in recipient cells, which was clearly greater than 1 after 24-h incubation (Figure 1B,C). Meanwhile, MCF7 cells showed a more rapid sEV capturing capability (Figure 1D), as evidenced by an increased abundance of sEV biomarkers (ALIX and CD63) in MCF7 cell membrane proteins after 6-h incubation, whereas a similar increase in MDA-MB-436 cells was only noted after 12-h incubation with the sEVs. The subsequent decrease in biomarkers after 24 h in both cell types suggested the sEVs were internalized in the recipient cells rather than remaining on the cell membrane (Figure 1E,F). Differences in sEV uptake preferences and kinetics were observed between MCF7 and MDA-MB-436 cells. Combined with previous findings of the preferential in vivo accumulation of sEVs and RNA-containing sEVs shed by stromal cells targeting basal/triple-negative breast cancer subtypes (Nabet et al. 2017; Xu et al. 2020), our results suggest that recipient cell-dependent selective sEV uptake is a biologically significant phenomenon.

3.2 | sEV Subpopulations Are Retrieved through Cell Fractionation of Recipient Cells

Next, to experimentally demonstrate the function-specific uptake of sEVs by recipient cells, we developed a method to retrieve and study sEV subpopulations from fractions of the intracellular membrane compartments of recipient cells. A coculture setup was employed to enhance both the population and heterogeneity of sEVs (Nabet et al. 2017). The retrieval was achieved through a

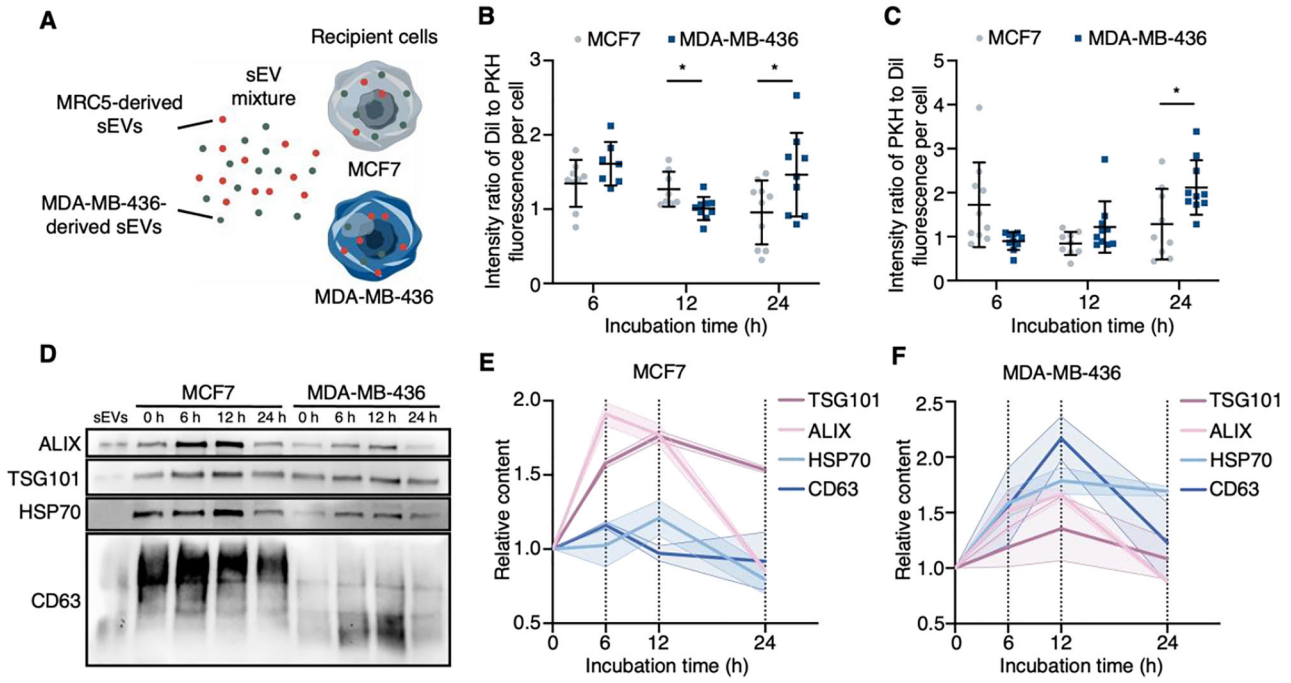

FIGURE 1 | Selective uptake of sEVs by MCF7 and MDA-MB-436 cells. (A) Schematic of the experiment conducted to observe selective uptake of sEVs derived from fibroblast (MRC5) and cancer (MDA-MB-436) cells by recipient cells (MCF7 and MDA-MB-436). (B) Fluorescence intensity ratios of sEVs derived from MRC5 and MDA-MB-436 cells in MCF7 and MDA-MB-436 cells, respectively. sEVs from MRC5 cells were labelled using red (DiI). sEVs from MDA-MB-436 cells were labelled using green (PKH) fluorescent dyes. (C) Fluorescence intensity ratios of sEVs derived from MRC5 and MDA-MB-436 cells in MCF7 and MDA-MB-436 cells, respectively. sEVs from MDA-MB-436 cells were labelled using red (DiI) and sEVs from MRC5 cells were labelled using green (PKH) fluorescent dyes. Each dot in (B and C) indicates the mean intensity ratio of MRC5 sEVs to MDA-MB-436 sEVs per cell from an independent experiment involving 200 cells. (D) Immunoblotting analysis of recipient cell membrane proteins after incubation with sEVs. Samples are normalized by total protein content, and sEV biomarkers (ALIX, TSG101, HSP70, CD63) are investigated. The image is representative of three trials. (E and F) Relative content of sEV biomarkers on the MCF7 (E) and MDA-MB-436 (F) cell membranes. Each data point represents the mean ± standard deviation (SD) from three independent experiments. *$p < 0.05$ by student's t-test.

cell fractionation process, which began with lysing the recipient cells via hypotonic treatment, followed by differential ultracentrifugation (dUC, Figure 2A). Given that the sEV uptake process actively depends on the type of recipient cells, the sEV dose, and the incubation time (Jurgielewicz et al. 2020), we introduced sEVs to the recipient cells to determine the best incubation time that enables us to efficiently isolate sEV subpopulations from recipient cells. First, the sEVs, isolated from the conditioned coculture medium of MRC5 and MDA-MB-436 cell mixtures, were stained with the stable cell membrane dye PKH67. These were then introduced to either MCF7 or MDA-MB-436 cells to determine the time at which most sEVs accumulated in the recipient cells. Fluorometric analysis validated an increase of sEVs in recipient cells during the initial 48 h, followed by a decrease at the 72-h point (Figure 2B,C). We directly lysed all the recipient cells without sorting those containing sEVs in their cytoplasm, as over 90% of the cells displayed sEVs within the cytoplasm (Figure 2D). We chose Triton X-100 as the primary reagent in the cell lysis buffer because it is a non-ionic detergent that selectively binds to hydrophobic regions of cell membranes and efficiently dissolves them while minimizing denaturation or loss of biological activity (Koval and Sprott 2014; Pryor 2014). To enable fast and efficient release of cell contents and prevent Triton X-100 from damaging sEVs from the recipient cell cytoplasm, we evaluated the performance of lysis buffers with varying concentrations of Triton X-100, and observed that a buffer with 0.1% Triton X-100 effectively disrupted cell membranes within 15 min (Figure 2E). Subsequently, sEV subpopulations from the recipient cell cytoplasm were isolated in the 100,000 g pellet of cell lysates through dUC. An increase in sEV biomarkers in the 100,000 g cell pellets of recipient cells after 48 h of incubation with the sEVs was observed by comparing immunoblotting results of cell pellets incubated for varying durations to those of control groups (MCF/MDA-MB-436 0 h) that underwent no sEV incubation (Figures 2F and S2), suggesting an existence of sEV biomarkers in recipient cell pellets. To further confirm that the detected biomarkers originated from internalized sEVs rather than from immature sEVs endogenously produced by the recipient cells, we treated the recipient cells with cycloheximide, a protein synthesis inhibitor, to minimize endogenous sEV biomarker expression. Even in the presence of cycloheximide, we observed an increase in ALIX levels in the recipient cell pellets after sEV incubation compared to the non-incubated controls, as shown in Figure S3. Besides, we also applied this sEV subpopulation retrieval method on mouse NIH/3T3 cells incubated with human-originated sEVs. The human sEV biomarker CD9 was detected in the 100,000 g cell pellet of mouse NIH/3T3 cells after incubation with these sEVs (Figure 2G). The time-dependent variation in sEV biomarkers and the presence of human sEV biomarkers in the mouse cell lysates confirmed that sEV subpopulations were internalized by recipient cells within 48 h and successfully recovered through the cell fractionation process.

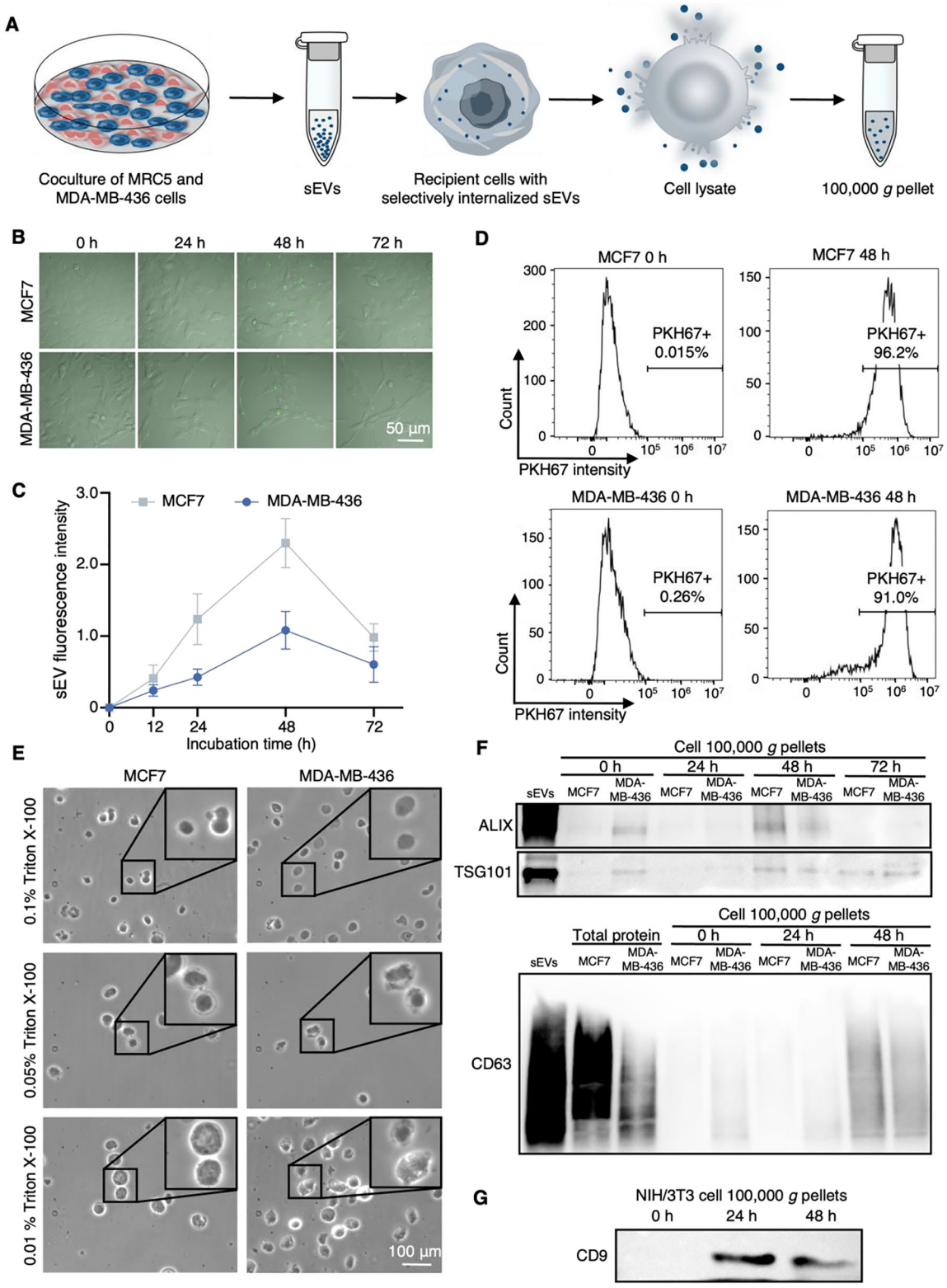

FIGURE 2 | Retrieval and characterization of internalized sEV subpopulations from recipient cells. (A) Schematic of the procedure for retrieving sEVs from recipient cells. (B) Confocal laser microscope images after incubation of MCF7 and MDA-MB-436 cells with sEVs. Equal amounts of sEVs (5×10^9 sEVs/mL) were labelled using hydrophobic lipid dye PKH67 and introduced to recipient cells for incubation periods of 0, 24, 48 and 72 h. Scale bar: 50 μm. (C) Quantification of fluorescence intensity associated with internalized sEVs in recipient cells after incubation with fluorescence-labelled sEVs for 0, 24, 48 and 72 h. Each data point represents the mean ± SD from three independent experiments. (D) Flow-cytometric enumeration of recipient cells containing green fluorescence-labelled sEVs. (E) Microscope observation of recipient cells after treatment with hypotonic lysis buffer containing varying concentrations of Triton X-100. (F) Immunoblotting analysis of sEV biomarkers in 100,000 *g* pellets of MCF7 and MDA-MB-436 cells after varying duration of sEV incubation. Samples are normalized by total protein content. See also Figure S2. (G) Immunoblotting analysis of human CD9 protein in mouse NIH/3T3 cells post-incubation with sEVs. Samples are normalized by total protein content. Immunoblotting images are representative of three trials.

To rigorously validate the retrieval method, we examined the sEV subpopulations in the 100,000 *g* cell pellets using multiple approaches with appropriate control groups. First, we analyzed the 100,000 *g* pellet for potential contamination from cellular contents such as lysosomes, ribosomes, endoplasmic reticula and endosomes, using corresponding biomarkers. Immunoblotting of total protein in these pellets also confirmed that the lysis buffer containing 0.1% Triton X-100 effectively released cellular compositions. However, it also increased contamination from endosomes and ribosomes (Figure 3A,B). Transmission electron microscopy (TEM, Figure 3C) and scanning electron microscopy (SEM, Figure S4) provided additional support for these findings while investigating the donut-shaped morphology of sEVs retrieved from recipient cells. TEM images revealed ribosome contaminants around 30 nm in size within the 100,000 *g* cell pellets. The sEV subpopulations retrieved from recipient cells after incubation with sEVs appeared as intact bilayer vesicles, resembling pure sEVs (Figure 3C, sEVs) with an approximate size of 100 nm, indicating successful recovery of sEVs that had been internalized by recipient cells but had not yet been degraded or undergone endosomal escape (Figure 3C, MCF/MDA-MB-436 48 h). The size of these sEVs was further verified to be around 100 nm using dynamic light scattering (DLS) and nanoparticle tracking analysis (NTA) (Figures 3D,E and S5). These findings further validate the successful retrieval of sEV subpopulations from recipient cells within the 100,000 *g* cell pellets.

3.3 | Retrieved sEV Subpopulations Exhibit Different Molecular Profiles

After validating the sEV subpopulation retrieval method, we next characterized selective uptake by comparing differences in the retrieved sEV subpopulations under various conditions. Due to the presence of contaminants detected in the retrieved sEV subpopulations, we incorporated 100,000 *g* pellets of recipient cells without sEV incubation (MCF7/MDA-MB-436 0 h) as appropriate control groups in the subsequent experiments. First, we examined the influence of sEV concentration on the retrieval rates of sEVs from different recipient cell types. Since the number of internalized sEVs reflects intrinsic differences among recipient cells and may correlate with selective uptake capacity, we analyzed sEV biomarker levels in the total protein of the 100,000 *g* cell pellets using immunoblotting. In MCF7 cells, the quantity of retrieved sEVs peaked at 7.5×10^{10} sEVs per 10^6 cells and declined at higher concentrations. In contrast, MDA-MB-436 cells showed a continued increase up to 15×10^{10} sEVs (Figure 4A). A similar trend was observed in lipid content assays for 100,000 *g* pellets of recipient cells with and without sEVs incubation (Figure 4B). These findings indicate that increasing the number of sEVs incubated with recipient cells does not always lead to higher retrieval rates. Instead, recipient cells appear to engage in a selective uptake process, suggesting an intrinsic discernment mechanism that regulates sEV internalization.

Next, we examined the concentration of sEV subpopulation within recipient cells relative to the total sEVs by measuring fluorescence intensity before and after cellular uptake. To mitigate potential false positive signals caused by PKH67 aggregation or transfer during cellular entry, we employed sEVs conjugated with Alexa 488 fluorophores through covalent bonding using bio-orthogonal click chemistry (Song et al. 2020; Dehghani et al. 2020), alongside those labelled with the hydrophobic dye PKH67. Both labelling methods showed that the fluorescence intensity from the retrieved sEVs constituted around 15% of the total sEVs in cases with MCF7 recipient cells and 10% in cases with MDA-MB-436 recipient cells (Figure 4C). This aligns with previous findings that the sEV uptake exhibits low yield (Bonsergent et al. 2021). However, low-yield uptake does not necessarily imply a minor effect on recipient cells, as initiating phenotypic alterations in recipient cells do not always need large quantities of molecules (Su et al. 2024).

We also investigated cargo differences among sEV subpopulations through protein and DNA electrophoresis, surface-enhanced Raman spectroscopy and immunoblotting. Given that the sEV subpopulations retrieved from the two different cell types were not pure, we used 100,000 *g* pellets of recipient cells without sEV incubation as control groups (MCF7/MDA-MB-436 0 h). The results from the cell pellets incubated with sEVs for 48 h were either compared directly to these control groups, or analyzed by subtracting or normalizing with the control values to evaluate differences between sEV subpopulations from the different cell types. We found that although the electrophoresis gel did not reveal distinct cargo differences (Figure S6), variations in lipid, protein and nucleic acid profiles were discerned by analyzing molecular vibration modes and Raman band assignments following the guidelines set out in MISEV2023 (Figure 4D) (Li et al. 2023; Stremersch et al. 2016; Welsh et al. 2024). After subtracting Raman signals originating from recipient cells, distinct Raman profiles were detected in the retrieved sEV subpopulations, indicating variations in molecular composition (Table S2) (Li et al. 2023; Stremersch et al. 2016). Meanwhile, we identified differential enrichment of sEV biomarkers in relative intensities measured through immunoblotting. For instance, TSG101 and ALIX were more prevalent in sEV subpopulations from MDA-MB-436 cells, whereas CD63 was more abundant in those from MCF7 cells, suggesting the selective uptake of the sEVs dependent on the types of cells (Figure 4E,F).

The observed differences in sEV accumulation, molecular profiles and protein enrichment suggest that recipient cells employ a selection mechanism when internalizing sEVs through endocytosis. The distinct cargo of these EVs is most likely to play a significant role in shaping their biological functions within recipient cells.

3.4 | Retrieved sEV Subpopulations Cause Different Phenotypic Responses on Cells

Given that sEVs are predominantly internalized through endocytosis and located within the cell cytoplasm, we applied two types of endocytosis inhibitors (Pitstop 2 and Filipin III) to recipient cells to examine the mechanisms underlying the accumulation of sEV subpopulations within recipient cells. Immunoblotting analysis showed that sEVs from cocultures increased in MCF7 cells but decreased in MDA-MB-436 cells after the endocytosis inhibitor treatments (Figure 5A). The inhibition of endocytosis may prevent MDA-MB-436 cells from uptaking sEVs and could trigger alternative uptake pathways in MCF7 cells. This result indicates intrinsic differences in the uptake mechanisms of

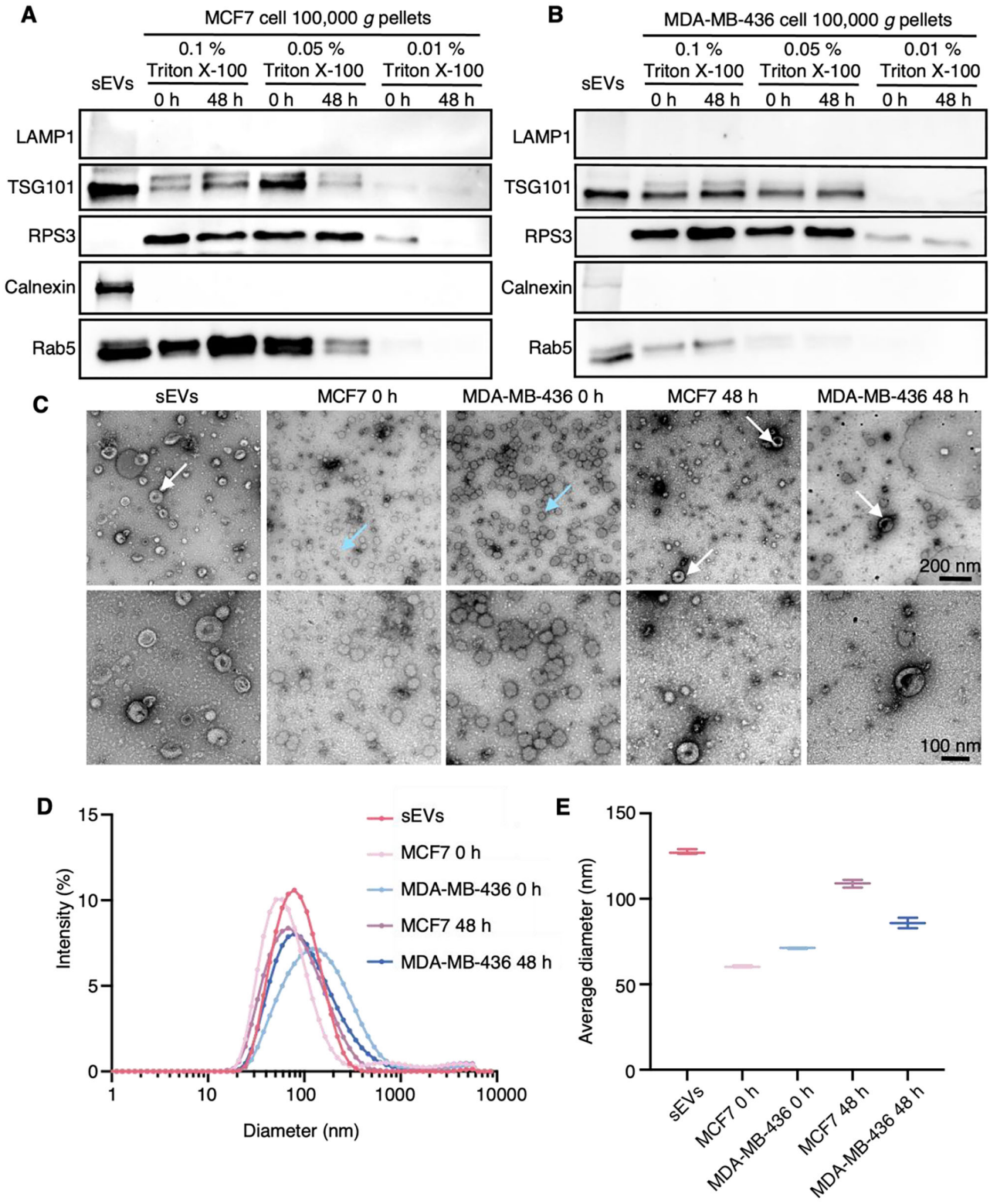

FIGURE 3 | Evaluation and validation of retrieved sEV subpopulations. (A and B) Immunoblotting analysis of LAMP1 (lysosomes), TSG101 (exosomes), RPS3 (ribosomes), Calnexin (endoplasmic reticulum) and Rab5 (endosomes) protein levels in 100,000 *g* pellets from MCF7 (A) and MDA-MB-436 (B) cells treated with varying concentrations of Triton X-100 after 48 h of sEV incubation compared to control groups without sEV incubation (0 h). Immunoblotting images are representative of three trials. Samples are normalized by total protein content. (C) TEM images showing donut-shaped sEVs in recipient cell pellets. Blue arrows indicate ribosomes and white arrows point to sEVs. Scale bars: 200 nm (upper), 100 nm (lower). See also Figure S4. (D and E) DLS analysis displaying the size distribution (D) and average diameter (E) of sEVs or 100,000 *g* pellets from recipient cells lysate, with (MCF7 48 h, MDA-MB-436 48 h) and without (MCF7 0 h, MDA-MB-436 0 h) sEV incubation. See also Figure S5. Each line represents the median; whiskers extend to the maximum and minimum values.

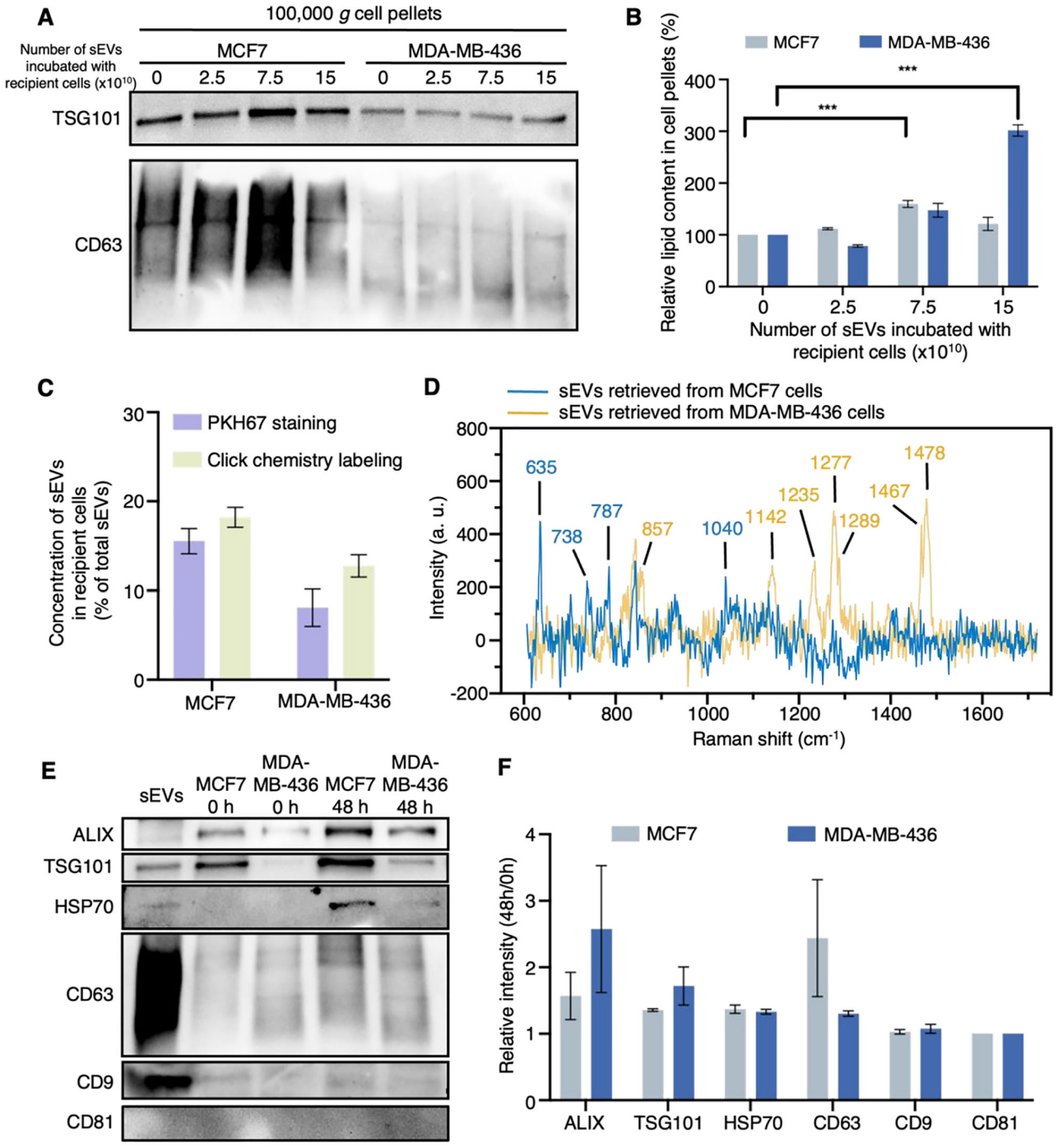

FIGURE 4 | Retrieved sEV subpopulations show distinct molecular profiles. (A) Immunoblotting analysis of sEV biomarkers (TSG101 and CD63) in 100,000 *g* pellets of MCF7 and MDA-MB-436 cells after 48 h incubation with varying numbers of sEVs (0 to 1.5×10^{11}). Samples are normalized by recipient cell numbers and total protein content. The image is representative of three trials. (B) Relative lipid content analysis of 100,000 *g* pellets of MCF7 and MDA-MB-436 cells after 48 h of incubation with varying numbers of sEVs, compared to control groups without sEV incubation. Samples are normalized by recipient cell numbers. Each data point represents the mean ± SD from three independent experiments. ***$p < 0.001$ by student's *t*-test. (C) Concentration ratios of the sEVs in recipient cell pellets compared to the total sEVs. sEVs were labelled by lipophilic (PKH67) or covalent bonded (click chemistry labelled Alexa 488) dyes. The proportion of sEV subpopulations compared to pre-incubation levels of sEVs was determined by their fluorescence intensity. (D) Raman spectroscopy of sEV subpopulations. Peaks of sEV subpopulations retrieved from MCF7 (MDA-MB-436) were obtained by subtracting the spectra of the control group pellets, MCF7 0 h (MDA-MB-436 0 h), from the spectra of MCF7 48 h (MDA-MB-436 48 h) cell pellets. See also Figure S6 and Table S1. (E) Immunoblotting analysis of sEV biomarkers in 100,000 *g* pellets of MCF7 and MDA-MB-436 cells incubated with sEVs for 48 h and without incubation (MCF7/MDA-MB-436 0 h). The analysis included cytosolic (ALIX, TSG101, HSP70) and transmembrane (CD63, CD9, CD81) proteins. Samples are normalized by total protein content. The image is representative of three trials. (F) Changes in sEV biomarkers in recipient cell pellets. Ratios represent levels of sEV biomarkers in recipient cells after sEV incubation (48 h) compared to controls without incubation (0 h). Each data point represents the mean ± SD from three independent experiments.

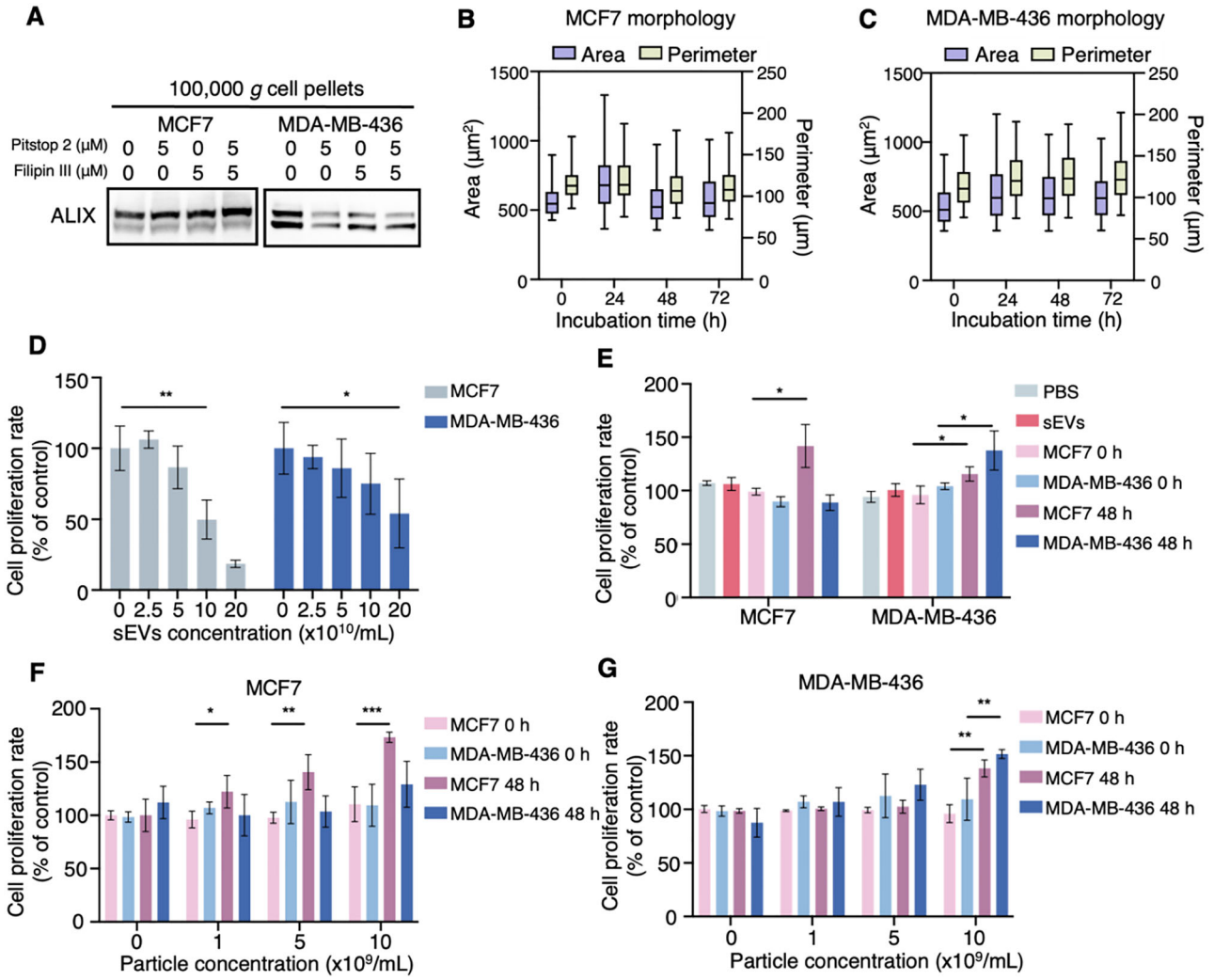

FIGURE 5 | Cell shape and proliferation regulated by sEV subpopulations. (A) Immunoblotting analysis of sEV content from recipient cells treated with pitstop 2 or filipin III. The sEV biomarker ALIX is shown as a representative maker of sEV content. The image is representative of three trials. Samples are normalized by total protein content. (B and C) Effects of coculture-derived sEV treatments on recipient cell morphology. See also Figure S1. Analyzed cells: $n = 200$. Each box represents the interquartile range; line within indicates the median; whiskers extend to the maximum and minimum values. (D) Dose-response of MCF7 and MDA-MB-436 cells to sEV treatments. Cell proliferation rates were compared to the control group treated with PBS. (E) Cell proliferation assessment of MCF7 and MDA-MB-436 cells after 24-h treatment with PBS, sEVs or recipient cell pellets with (MCF7/MDA-MB-436 48 h) and without (MCF7/MDA-MB-436 0 h) sEV incubation. Cells were treated with the same number of particles. (F) Dose-response analysis for MCF7 cells treated with various concentrations of recipient cell pellets with (MCF7/MDA-MB-436 48 h) and without (MCF7/MDA-MB-436 0 h) sEV incubation. (G) Dose-response analysis for MDA-MB-436 cells treated with various concentrations of recipient cell pellets with (MCF7/MDA-MB-436 48 h) and without (MCF7/MDA-MB-436 0 h) sEV incubation. Each data point represents the mean ± SD from three independent experiments. $^{*}p < 0.05$, $^{**}p < 0.01$ and $^{***}p < 0.001$ by student's *t*-test.

MCF7 and MDA-MB-436 cells, which are closely related to the cargoes and biological functions of the sEV subpopulations in the recipient cells.

The primary role of sEVs is to transfer substances from donor to recipient cells, which can subsequently alter gene expression and affect signalling pathways (Melo et al. 2014; Rajagopal and Harikumar 2018; Nishimura et al. 2021). Therefore, evaluating sEV functions requires considering not only the cargo of the sEVs but also the characteristics of their recipient cells. To this end, we performed various functional assays of sEV subpopulations on both recipient and non-recipient cells to explore differences among the sEVs and their subpopulations. In the beginning, we found that sEV subpopulations caused no significant morphological changes in their recipient cells according to microscopic observations (Figures 5B,C and S1), although their cell proliferation rate decreased in a dose-dependent manner (Figure 5D).

Next, we incubated sEV subpopulations retrieved from recipient cells with new sets of MCF7 or MDA-MB-436 cells and compared their effects to verify their distinct functions on cells, such as phenotypic reprogramming. Pure cytoplasmic contents isolated from recipient cells without sEV incubation (MCF7/MDA-MB-436 0 h) served as control groups. Cell proliferation analysis indicated that sEVs obtained from MCF7 cells notably enhanced MCF7

cell growth, yet had minimal impact on MDA-MB-436 cells, and vice versa (Figure 5E). A similar trend was observed in the dose-response assessments of sEV subpopulations (Figure 5F,G).

Moreover, we further underscored the distinct functionalities of sEVs on phenotypic changes in cells. Specifically, sEV subpopulations retrieved from both MCF7 cells and MDA-MB-436 cells significantly enhanced migration in both cell types (Figure 6A,B). This suggests that the migration effect, which was subtle when heterogeneous sEVs were directly incubated with the two types of cells ('sEVs' in Figure 6A,B), became pronounced when specific sEV subpopulations retrieved from recipient cells were applied. Similarly, we identified that sEVs retrieved from MDA-MB-436 cells accelerated colony formation in cells, regardless of the cell type, while those from MCF7 cells had little or even a negative impact (Figure 6C). The clonogenic potential, indicative of tumour cell viability at new metastatic sites, was influenced differently by these sEV subpopulations. On the other hand, we evaluated the expression of key biomarkers that dictate cell fate and found that sEV subpopulations affected stemness (NOTCH3, EpCAM), cell adhesion and migration (EpCAM, E-cadherin), autophagy (LC3B) and immune resistance (PD-L1) in cells in different ways (Figure 6D,E). For example, the sEV subpopulation retrieved from MCF7 recipient cells significantly increased PD-L1 expression in MCF7 cells, enhancing immune evasion, whereas that from MDA-MB-436 recipient cells significantly reduced E-cadherin expression in MDA-MB-436 cells, promoting cell migration. Additionally, the sEV subpopulation retrieved from MDA-MB-436 recipient cells enhanced LC3B levels and reduced E-cadherin expression regardless of the type of cells. However, their impact on NOTCH3 expression varied depending on the type of cells, reflecting inherent differences between recipient cell types.

In addition to cancer cells, we also evaluated the functionalities of the sEV subpopulations on normal fibroblast cells (MRC5) to explore their potential influence and applications, such as their role in modulating normal cell behaviour. Cell proliferation (Figure S7A) and migration assays (Figure S7B,C) indicated that sEVs retrieved from MCF7 cells caused minimal impact on MRC5 cells, whereas sEVs retrieved from MDA-MB-436 cells significantly inhibit MRC5 proliferation and migration. This effect was also reflected in the expression of the NOTCH3 protein in MRC5 cells (Figure S7D), with sEVs from MDA-MB-436 cells showing a marked suppressive effect, while sEVs retrieved from MCF7 cells caused only a slight reduction. These results suggest that sEV subpopulations retrieved from MDA-MB-436 cells may function as suppressors of fibroblast proliferation and migration. Taken together, these findings strongly indicate that the sEV subpopulations we retrieved from different recipient cells exhibit distinct functional characteristics that influence the activities of cells.

4 | Discussion

It is well known that cells generate heterogeneous sEVs carrying diverse cargoes that deliver biological information and impart specific functions to recipient cells (Pluchino and Smith 2019), particularly those originating from multivesicular bodies, such as exosomes, which undergo context-specific regulation of cargo sorting processes (Dixson et al. 2023). However, due to the extreme heterogeneity of sEVs and the complexity of cellular interactions, it remains unclear whether sEVs with specific functions consistently reach their intended destinations. In this study, we provided direct experimental evidence supporting the hypothesis that recipient cells selectively internalize sEVs based on their functional properties. Our strategy consisted of two components: (1) the development and validation of a crude extraction method for isolating internalized sEV subpopulations from the intracellular membrane compartments of recipient cells and (2) the functional analysis of these sEV subpopulations to assess their biological influence on recipient cells.

For part 1, we employed breast cancer cells with varying degrees of malignancy and different surface receptors (ER, PR, HER2) as recipient cells. This variation provided a valuable model to investigate the precision with which cells can distinguish and take up specific sEVs. As endocytosis serves as the primary mechanism for sEV uptake, our focus was on retrieving those sEVs that had been selectively internalized by recipient cells. Given the lack of a standard protocol for isolating internalized sEVs, we developed a streamlined cell fractionation method based on hypotonic treatment and dUC. This method, however, inevitably leads to contamination from cytoplasmic components of recipient cells. Therefore, MCF7 and MDA-MB-436 cells, without sEV incubation, served as control groups. In line with MISEV2023 guidelines for sEV characterization (Welsh et al. 2024), our findings, including elevated amounts of sEV biomarkers in both human and mouse recipient cells lysates (Figure 2F,G), direct observation of sEV morphology (Figures 3C and S4), and fluorescence tracing before and after the sEV incubation (Figure 4C), suggest that despite the presence of impurities in the 100,000 *g* cell pellets, distinct subpopulations of sEVs are clearly evident.

For part 2, to elucidate the functions of sEV subpopulations retrieved from the recipient cells, we assessed their cargoes and observed subsequent phenotype alterations in cells after the treatment with these retrieved sEV subpopulations. Our data revealed distinct molecular and protein profiles within the sEV subpopulations after their retrieval (Figure 4D–F). Additionally, the functional assays conducted on cells further confirmed these distinct functional identities (Figure 6). Notably, sEV subpopulations obtained from specific recipient cell types significantly enhanced the cell proliferation rate and tumourigenicity of those same cell types (Figures 5E and 6A–C). The disparities in their impacts on molecular-level changes in cells were substantial (Figure 6D,E). These findings suggest that recipient cells employ a function-based selection mechanism when internalizing sEVs from the environment (Figure 7). The functional impact of sEVs appears to be dependent on the type of recipient cells, and this phenomenon particularly evident among different breast cancer subtypes.

However, certain challenges and questions persist. First, the lack of well-established methods for isolating external sEVs from recipient cell cytoplasm, necessitated the use of a relatively simple, albeit crude, approach to retrieve post-uptake sEV subpopulations. As a result, these subpopulations were found to carry various contaminants such as ribosomes and endosomes. Additionally, all recipient cells may simultaneously generate and internalize sEVs, leading to a mixed population of sEVs that

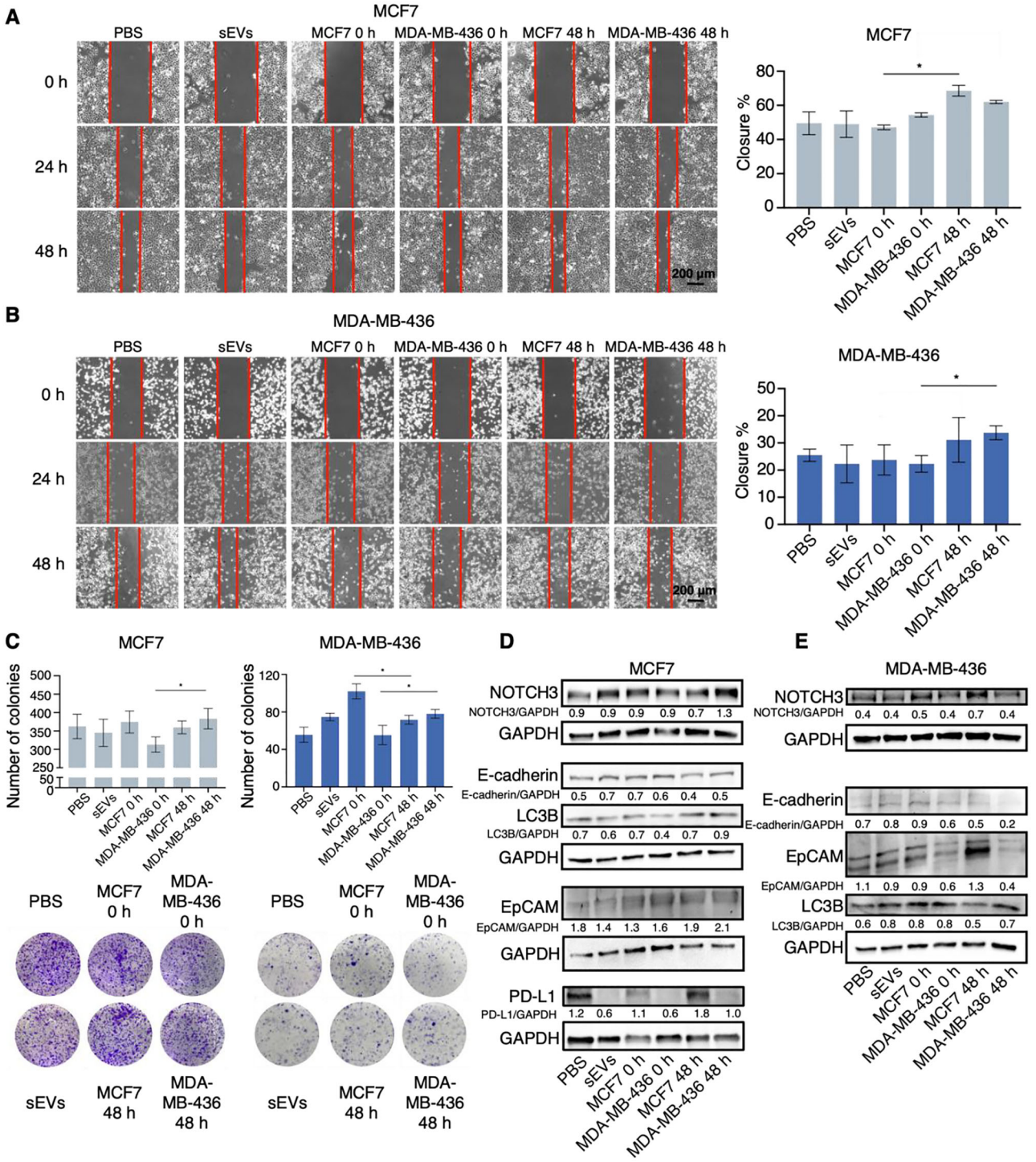

FIGURE 6 | Cell migration, clonogenicity and protein expression modulated by sEV subpopulations. (A) Scratch assay and closure analysis of MCF7 cells treated with PBS, sEVs and recipient cell pellets with (MCF7/MDA-MB-436 48 h) and without (MCF7/MDA-MB-436 0 h) sEV incubation. (B) Scratch assay and closure analysis of MDA-MB-436 cells treated with PBS, sEVs or recipient cell pellets with (MCF7/MDA-MB-436 48 h) and without (MCF7/MDA-MB-436 0 h) sEV incubation. Scale bars: 200 μm. (C) Colony formation outcomes for MCF7 and MDA-MB-436 cells treated with PBS, sEVs or recipient cell pellets with (MCF7/MDA-MB-436 48 h) and without (MCF7/MDA-MB-436 0 h) sEV incubation. (D) Immunoblotting analysis illustrating changes in NOTCH3, E-cadherin, LC3B, EpCAM and PD-L1 expression in MCF7 cells after 48 h of treatments with PBS, sEVs or recipient cell pellets with (MCF7/MDA-MB-436 48 h) and without (MCF7/MDA-MB-436 0 h) sEV incubation. (E) Immunoblotting analysis showing NOTCH3, E-cadherin, EpCAM and LC3B expression in MDA-MB-436 cells after 48 h of treatments with PBS, sEVs or recipient cell pellets with (MCF7/MDA-MB-436 48 h) and without (MCF7/MDA-MB-436 0 h) sEV incubation. Each data point represents the mean ± SD from three independent experiments; immunoblotting images are representative of three trials. *$p < 0.05$ by student's *t*-test.

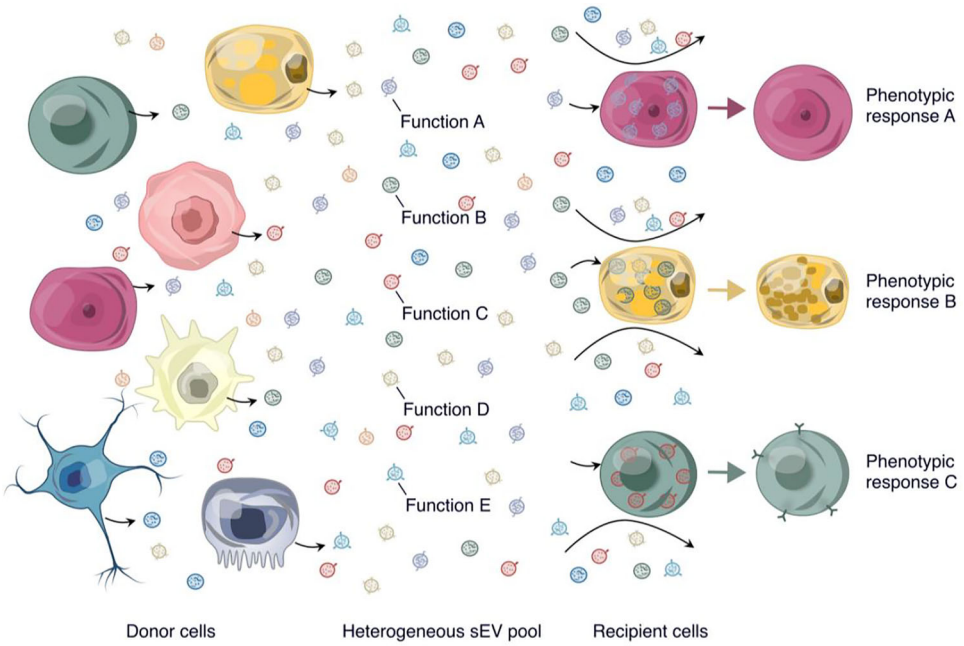

FIGURE 7 | Concept of function-specific uptake of sEVs by recipient cells. Donor cells of varying types secrete a highly heterogeneous population of sEVs, each carrying distinct bioactive molecules. Recipient cells, based on their unique biological needs and conditions, selectively internalize function-specific sEVs. This selective uptake leads to diverse phenotypic responses in different types of recipient cells, influencing their behaviour, signalling pathways and overall cellular function.

consists of both endogenously generated and externally sourced sEVs (Kalluri and LeBleu 2020). This complicates the functional analysis of these subpopulations. Second, in our validation of functional differences, we re-incubated the sEV subpopulations mixed with cytoplasm contaminations with different recipient cells. These cells then might selectively internalize these contaminations, potentially introducing biases in our assessment of sEV functionalities.

In conclusion, our results provide direct experimental evidence that recipient cells selectively uptake function-specific sEVs from their environment. This finding lays a crucial foundation for further investigation into the specificity of sEV-cell interactions. This foundational knowledge enhances the understanding of exploring how sEV-mediated communication influences cellular behaviour in both health and disease. Further investigation into this mechanism may shed light on the molecular basis of cell discernment and critical processes in intercellular communication, with implications for understanding disease progression and developing therapeutic strategies.

Author Contributions

Yuhong Liu: conceptualization, methodology, investigation, visualization, funding acquisition, project administration, writing–original draft, writing–review and editing. **Natsumi Tiffany Ishii**: methodology, writing–review and editing. **Jun-Yu Dong**: methodology, visualization, writing–review and editing. **Yaqi Zhao**: methodology, writing–review and editing. **Yingdong Luo**: methodology, visualization, writing–review and editing. **Zhuhui Ren**: methodology, writing–review and editing. **Tianben Ding**: conceptualization, investigation, funding acquisition, supervision, writing–original draft, writing–review and editing. **Tamako Nishimura**: methodology, writing–review and editing. **Ryo Iizuka**: writing–review and editing. **Akihiro Isozaki**: conceptualization, writing–review and editing. **Sotaro Uemura**: writing–review and editing. **Shiro Suetsugu**: conceptualization, writing–review and editing. **Keisuke Goda**: conceptualization, funding acquisition, supervision, writing–review and editing.

Acknowledgements

We thank the staff in the FACS Core Laboratory at the University of Tokyo. We also extend our gratitude to Serendipity Lab for facilitating collaboration opportunities. This work was mainly supported by JSPS Core-to-Core Program JPJSCCCA20190007 (K.G.), JSPS KAKENHI JP20H00317 (K.G.), JP23KJ0430 (Y.L.), JP24K17800 (T.D.), JP23H02476 (T.N.), JP24H01286 and JP24K02024 (S.S.), JST ASPIRE Program JPMJAP2316 (K.G.), JST CREST JPMJCR1863 and JPMJCR24B3 (S.S.), Mazda Foundation (T.D.) and KAKETSUKEN (K.G.). Additional support was provided by supported by the Mohammed bin Salman Center for Future Science and Technology for Saudi-Japan Vision 2030 (K.G.), the Cell Aging Control Endowed Chair at the University of Tokyo (K.G.) and the Nanotechnology Platform Project by the Ministry of Education, Culture, Sports, Science and Technology of Japan JPMXP09A21UT0014.

Conflicts of Interest

Keisuke Goda is a shareholder of CYBO and FlyWorks, Inc.

Data Availability Statement

The data that support the findings of this study are available from the corresponding author upon reasonable request.

References

Ben-Aicha, S., M. Anwar, G. Vilahur, et al. 2024. "Small Extracellular Vesicles in the Pericardium Modulate Macrophage Immunophenotype in Coronary Artery Disease." *JACC: Basic to Translational Science* 9: 1057–1072.

Bonsergent, E., E. Grisard, J. Buchrieser, O. Schwartz, C. Théry, and G. Lavieu. 2021. "Quantitative Characterization of Extracellular Vesicle Uptake and Content Delivery Within Mammalian Cells." *Nature Communications* 12: 1864.

Bordanaba-Florit, G., F. Royo, S. G. Kruglik, and J. M. Falcón-Pérez. 2021. "Using Single-Vesicle Technologies to Unravel the Heterogeneity of Extracellular Vesicles." *Nature Protocols* 16: 3163–3185.

Chen, G., A. C. Huang, W. Zhang, et al. 2018. "Exosomal PD-L1 Contributes to Immunosuppression and Is Associated With Anti-PD-1 Response." *Nature* 560: 382–386.

Cheng, F., Z. Wang, G. You, Y. Liu, J. He, and J. Yang. 2023. "Osteocyte-Derived Exosomes Confer Multiple Myeloma Resistance to Chemotherapy Through Acquisition of Cancer Stem Cell-Like Features." *Leukemia* 37: 1392–1396.

Costa Verdera, H., J. J. Gitz-Francois, R. M. Schiffelers, and P. Vader. 2017. "Cellular Uptake of Extracellular Vesicles Is Mediated by Clathrin-Independent Endocytosis and Macropinocytosis." *Journal of Controlled Release* 266: 100–108.

Dehghani, M., S. M. Gulvin, J. Flax, and T. R. Gaborski. 2020. "Systematic Evaluation of PKH Labelling on Extracellular Vesicle Size by Nanoparticle Tracking Analysis." *Scientific Reports* 10: 9533.

Dixson, A. C., T. R. Dawson, D. Di Vizio, and A. M. Weaver. 2023. "Context-Specific Regulation of Extracellular Vesicle Biogenesis and Cargo Selection." *Nature Reviews Molecular Cell Biology* 24: 454–476.

Fuentes, P., M. Sesé, P. J. Guijarro, et al. 2020. "ITGB3-Mediated Uptake of Small Extracellular Vesicles Facilitates Intercellular Communication in Breast Cancer Cells." *Nature Communications* 11: 4261.

He, B., H. Wang, G. Liu, et al. 2023. "Fungal Small RNAs Ride in Extracellular Vesicles to Enter Plant Cells Through Clathrin-Mediated Endocytosis." *Nature Communications* 14: 4383.

Hoshino, A., B. Costa-Silva, T.-L. Shen, et al. 2015. "Tumour Exosome Integrins Determine Organotropic Metastasis." *Nature* 527: 329–335.

Ivanova, A., L. Badertscher, G. O'Driscoll, et al. 2023. "Creating Designer Engineered Extracellular Vesicles for Diverse Ligand Display, Target Recognition, and Controlled Protein Loading and Delivery." *Advanced Science* 10: 2304389.

Jurgielewicz, B. J., Y. Yao, and S. L. Stice. 2020. "Kinetics and Specificity of HEK293T Extracellular Vesicle Uptake Using Imaging Flow Cytometry." *Nanoscale Research Letters* 15: 170.

Kalluri, R., and V. S. LeBleu. 2020. "The Biology, Function, and Biomedical Applications of Exosomes." *Science (1979)* 367: eaau6977.

Koval, S. F., and G. D. Sprott. 2014. "Cell Fractionation." In *Methods for General and Molecular Microbiology*, 108–137. ASM Press.

Kowal, J., G. Arras, M. Colombo, et al. 2016. "Proteomic Comparison Defines Novel Markers to Characterize Heterogeneous Populations of Extracellular Vesicle Subtypes." *Proceedings of the National Academy of Sciences* 113: E968–E977.

Li, X., M. Keshavarz, P. Kassanos, et al. 2023. "SERS Detection of Breast Cancer-Derived Exosomes Using a Nanostructured Pt-Black Template." *Advanced Sensor Research* 2: 2200039.

Mathieu, M., L. Martin-Jaular, G. Lavieu, and C. Théry. 2019. "Specificities of Secretion and Uptake of Exosomes and Other Extracellular Vesicles for Cell-to-Cell Communication." *Nature Cell Biology* 21: 9–17.

Melo, S. A., H. Sugimoto, J. T. O'Connell, et al. 2014. "Cancer Exosomes Perform Cell-Independent MicroRNA Biogenesis and Promote Tumorigenesis." *Cancer Cell* 26: 707–721.

Montecalvo, A., A. T. Larregina, W. J. Shufesky, et al. 2012. "Mechanism of Transfer of Functional MicroRNAs Between Mouse Dendritic Cells via Exosomes." *Blood* 119: 756–766.

Mulcahy, L. A., R. C. Pink, and D. R. F. Carter. 2014. "Routes and Mechanisms of Extracellular Vesicle Uptake." *Journal of Extracellular Vesicles* 3: 24641.

Nabet, B. Y., Y. Qiu, J. E. Shabason, et al. 2017. "Exosome RNA Unshielding Couples Stromal Activation to Pattern Recognition Receptor Signaling in Cancer." *Cell* 170: 352–366.e13.

Nishimura, T., T. Oyama, H. T. Hu, et al. 2021. "Filopodium-Derived Vesicles Produced by MIM Enhance the Migration of Recipient Cells." *Developmental Cell* 56: 842–859.e8.

Peruzzi, J. A., T. F. Gunnels, H. I. Edelstein, et al. 2024. "Enhancing Extracellular Vesicle Cargo Loading and Functional Delivery by Engineering Protein-Lipid Interactions." *Nature Communications* 15: 5618.

Pluchino, S., and J. A. Smith. 2019. "Explicating Exosomes: Reclassifying the Rising Stars of Intercellular Communication." *Cell* 177: 225–227.

Pryor, P. R. 2014. Subcellular Fractionation: A Laboratory Manual. Cold Spring Harbor Laboratory Press: p27–40.

Qiu, Y., Y. Yang, R. Yang, et al. 2021. "Activated T Cell-Derived Exosomal PD-1 Attenuates PD-L1-Induced Immune Dysfunction in Triple-Negative Breast Cancer." *Oncogene* 40: 4992–5001.

Rajagopal, C., and K. B. Harikumar. 2018. "The Origin and Functions of Exosomes in Cancer." *Frontiers in Oncology* 8: 66.

Rilla, K. 2021. "Diverse Plasma Membrane Protrusions Act as Platforms for Extracellular Vesicle Shedding." *Journal of Extracellular Vesicles* 10: e12148.

Song, M., L. Tong, S. Liu, et al. 2021. "Nonlinear Amplification of Chirality in Self-Assembled Plasmonic Nanostructures." *ACS Nano* 15: 5715–5724.

Song, S., M. K. Shim, S. Lim, et al. 2020. "In Situ One-Step Fluorescence Labeling Strategy of Exosomes via Bioorthogonal Click Chemistry for Real-Time Exosome Tracking In Vitro and In Vivo." *Bioconjugate Chemistry* 31: 1562–1574.

Stremersch, S., M. Marro, B.-E. Pinchasik, et al. 2016. "Identification of Individual Exosome-Like Vesicles by Surface Enhanced Raman Spectroscopy." *Small* 12: 3292–3301.

Stringer, C., T. Wang, M. Michaelos, and M. Pachitariu. 2021. "Cellpose: A Generalist Algorithm for Cellular Segmentation." *Nature Methods* 18: 100–106.

Su, J., Y. Song, Z. Zhu, et al. 2024. "Cell–Cell Communication: New Insights and Clinical Implications." *Signal Transduction and Targeted Therapy* 9: 196.

Sung, B. H., C. A. Parent, and A. M. Weaver. 2021. "Extracellular Vesicles: Critical Players During Cell Migration." *Developmental Cell* 56: 1861–1874.

Théry, C., S. Amigorena, G. Raposo, and A. Clayton. 2006. "Isolation and Characterization of Exosomes From Cell Culture Supernatants and Biological Fluids." *Current Protocols in Cell Biology* 30: 3.22.1–3.22.29.

Tosar, J. P., F. Gambaro, J. Sanguinetti, B. Bonilla, K. W. Witwer, and A. Cayota. 2015. "Assessment of Small RNA Sorting Into Different Extracellular Fractions Revealed by High-Throughput Sequencing of Breast Cell Lines." *Nucleic Acids Research* 43: 5601–5616.

Urabe, F., N. Kosaka, Y. Yamamoto, et al. 2023. "Metastatic Prostate Cancer-Derived Extracellular Vesicles Facilitate Osteoclastogenesis by Transferring the CDCP1 Protein." *Journal of Extracellular Vesicles* 12: e12312.

van de Wakker, S. I., F. M. Meijers, J. P. G. Sluijter, and P. Vader. 2023. "Extracellular Vesicle Heterogeneity and Its Impact for Regenerative Medicine Applications." *Pharmacological Reviews* 75: 1043–1061.

van Niel, G., G. D'Angelo, and G. Raposo. 2018. "Shedding Light on the Cell Biology of Extracellular Vesicles." *Nature Reviews Molecular Cell Biology* 19: 213–228.

Wang, Y.-Z., C. C. M. Castillon, K. K. Gebis, et al. 2024. "Notch Receptor-Ligand Binding Facilitates Extracellular Vesicle-Mediated Neuron-to-Neuron Communication." *Cell Reports* 43: 113680.

Welsh, J. A., D. C. I. Goberdhan, L. O'Driscoll, et al. 2024. "Minimal Information for Studies of Extracellular Vesicles (MISEV2023): From Basic to Advanced Approaches." *Journal of Extracellular Vesicles* 13: e12404.

Wen, S. W., J. Sceneay, L. G. Lima, et al. 2016. "The Biodistribution and Immune Suppressive Effects of Breast Cancer–Derived Exosomes." *Cancer Research* 76: 6816–6827.

Xu, L., F. N. Faruqu, R. Liam-or, et al. 2020. "Design of Experiment (DoE)-Driven *In Vitro* and *In Vivo* Uptake Studies of Exosomes for Pancreatic Cancer Delivery Enabled by Copper-Free Click Chemistry-Based Labelling." *Journal of Extracellular Vesicles* 9: 1779458.

Yu, W., J. Hurley, D. Roberts, et al. 2021. "Exosome-Based Liquid Biopsies in Cancer: Opportunities and Challenges." *Annals of Oncology* 32: 466–477.

Zomer, A., C. Maynard, F. J. Verweij, et al. 2015. "In Vivo Imaging Reveals Extracellular Vesicle-Mediated Phenocopying of Metastatic Behavior." *Cell* 161: 1046–1057.

Supporting Information

Additional supporting information can be found online in the Supporting Information section.

Supplementary Materials: jex270088-sup-0001-SuppMat.docx